

Computational Analysis of a Generic Bell 206B Helicopter Tail Rotor Blade using ANSYS FLUENT

Firdaus^a, Jaswar Koto^{a,b,*}, I.S. Ishak^a and M.S. Ammoo^a

^aDepartment of Aeronautical, Automotive and Ocean Engineering, Faculty of Mechanical Engineering, Universiti Teknologi Malaysia

^bOcean and Aerospace Engineering Research Institute, Indonesia

*Corresponding author: jaswar@fkm.utm.my and jaswar.koto@gmail.com

Paper History

Received: 15-May-2015

Received in revised form: 18-May-2015

Accepted: 19-May-2015

ABSTRACT

This paper presents the computational analysis of three dimensional (3D) flow over the generic model of Bell 206B helicopter tail rotor blades using ANSYS Fluent Computational Fluid Dynamics (CFD) package. This simulation work deals with the comparative study of variation in an angle of attack over the blade at different speed which using the $k-\omega$ shear stress transport (SST) model. The model is utilized to predict the flow accurately along with turbulence intensities 5% and 5% at velocity inlet and pressure outlet respectively. The meshing 3D geometry was performed on ICEM CFD package of ANSYS and the simulation was executed in the FLUENT package of ANSYS. The simulation results were validated by comparing with the experimental result that have already done before.

KEY WORDS: *NACA 0012; lift coefficient (C_L); drag coefficient (C_D); helicopter tail rotor blades; Bell B206; $k-\omega$ shear stress transport (SST) model; FLUENT.*

NOMENCLATURE

C_L	Lift coefficient
C_D	Drag coefficient
CFD	Computational Fluid Dynamic
DES	Detached Eddy Simulation
SST	Shear Stress Transport

1.0 INTRODUCTION

The propeller blade is the device that mainly used as propulsive for marine vehicles, airplanes and rotorcraft. As it is a crucial part, it has to be designed to meet power requirement at the indicated speed with optimum efficiency. Now days, with growing demands for of higher speed and greater power, the propeller is becoming increasingly larger in size and its geometry shape become more complicated. Due this complicated geometry, the propeller should be optimally designed for increased propulsion efficiency.

To predict the steady and unsteady propeller characteristics, many numerical models for propeller blade simulation were proposed.

Recently, advanced Reynolds Averaged Navier Stokes (RANS) equations are well known for numerically predicting fully turbulent part of the flow field. Even though much accomplishment has been achieved, essential problem still exists where the standard fully turbulent RANS approach fail to give sufficiently accurate results (Niels N. Srensen, 2009). This problem is due to, none of these models are sufficient to handle flows with significant transition effects because of lack of practical transition modeling (Ünver Kaynak, 2012). Nevertheless, transition predictions have shown certain progress and utility by means of the well-known e^N method (Giles, 1987), some two-equation low Re-number turbulence models (Wilcox, 1994), and some methods based on experimental correlations (Suzen, 2000).

The new correlation based $\gamma-Re_\theta$ model (Menter et al., 2004) and the Detached Eddy Simulation (DES) version of the $k-\omega$ SST model (Strelets, 2001) is applied, in order to execute the flow simulations. It is well known that the movement of the separation point on the airfoil is highly influenced by the laminar to turbulent transition process. Furthermore, it is well known that typical RANS are not sufficiently accurate in massively separated flows, and the DES technique is applied to solve this problem.

In this study, 3-D computational result was obtained using the FLUENT software for a generic model of Bell 206B helicopter tail

rotor blade airfoil. The aim of this study is to investigate the prediction of aerodynamic characteristics of the tail rotor blades. The $k-\omega$ shear stress transport (SST) transition model are used in conjunction with the build-in Reynolds-averaged Navier-Stokes (RANS) solver. The results were compared with the results gathered from previous experiment of a full-scaled generic model of Bell 206B helicopter tail rotor blade, conducted in the Universiti Teknologi Malaysia- Low Speed Tunnel (Firdaus, 2015).

2.0 THEORETICAL FORMULATIONS NUMERICAL METHOD

2.1 The $k-\omega$ Shear Stress Transport (SST) Model

This model was implemented from two-equation Eddy-Viscosity turbulence models that were developed by Menter, F. R. (1994) to efficiently blend the vigorous and precise formulation of the $k-\omega$ standard model in the near-wall region with the free-stream liberation of the $k-\omega$ standard model in the far field. This is achieved by the conversion of the $k-\omega$ standard model into a $k-\omega$ formulation (Tousif Ahmed, 2013). The $k-\omega$ SST model is comparable to the standard $k-\omega$ model, but following improvement are included:

- Both the standard $k-\omega$ model and the transformed $k-\omega$ model was multiplied by a blending function and both models are added together after that. The blending function is the one activating the standard $k-\omega$ model in the near-wall region, and it is zero away from the surface, which activates the transformed $k-\omega$ model.
- The SST model integrated a damped cross-diffusion derivative term in the ω equation.
- The transport of the turbulent shear stress is accounted from the turbulent viscosity definition that has been modified.
- The modeling constants are made different.

These features make the SST $k-\omega$ model more accurate and reliable for a wider class of flows (e.g., adverse pressure gradient flows, airfoils, and transonic shock waves) compared to the standard $k-\omega$ model. SST $k-\omega$ model is given by the following:

$$\frac{\partial(\rho k)}{\partial t} + \frac{\partial(\rho u_j k)}{\partial x_j} = P - \beta^* \rho \omega k + \frac{\partial}{\partial x_j} \left[(\mu + \sigma_k \mu_t) \frac{\partial k}{\partial x_j} \right] \quad (1)$$

$$\frac{\partial(\rho \omega)}{\partial t} + \frac{\partial(\rho u_j \omega)}{\partial x_j} = \frac{\gamma}{v_t} P - \beta \rho \omega^2 + \frac{\partial}{\partial x_j} \left[(\mu + \sigma_\omega \mu_t) \frac{\partial \omega}{\partial x_j} \right] + 2(1 - F_1) \frac{\rho \sigma_{\omega 2}}{\omega} \frac{\partial k}{\partial x_j} \frac{\partial \omega}{\partial x_j} \quad (2)$$

Where

$$P = \tau_{ij} \frac{\partial \mu_i}{\partial x_j}$$

$$\tau_{ij} = \mu_t \left(2S_{ij} - \frac{2}{3} \frac{\partial \mu_k}{\partial x_k} \delta_{ij} \right) - \frac{2}{3} \rho k \delta_{ij}$$

$$S_{ij} = \frac{1}{2} \left(\frac{\partial \mu_i}{\partial x_j} + \frac{\partial \mu_j}{\partial x_i} \right)$$

and the turbulent eddy viscosity can be shown as:

$$\mu_t = \frac{\rho \alpha_1 k}{\max(\alpha_1 \omega, \Omega F_2)} \quad (3)$$

An inner (1) and outer (2) constant was blended for each of the constants are done by:

$$\phi = F_1 \phi_1 + (1 - F_1) \phi_2 \quad (4)$$

Where ϕ_1 is constant 1 and ϕ_2 is constant 2. And the other functions are given by:

$$F_1 = \tanh(\text{arg}_1^4)$$

$$\text{arg}_1 = \min \left[\max \left(\frac{\sqrt{k}}{\beta^* \omega d}, \frac{500\nu}{d^2 \omega} \right), \frac{4\rho \omega_2 k}{CD_{k\omega} d^2} \right]$$

$$CD_{k\omega} = \max \left(2\rho \sigma_{\omega 2} \frac{1}{\omega} \frac{\partial k}{\partial x_j} \frac{\partial \omega}{\partial x_j}, 10^{-20} \right)$$

$$F_2 = \tanh(\text{arg}_2^2)$$

$$\text{arg}_2 = \max \left[2 \frac{\sqrt{k}}{\beta^* \omega d}, \frac{500\nu}{d^2 \omega} \right]$$

Where ρ is the density, $\nu_t = \mu_t / \rho$ is the turbulent kinematic viscosity, μ is the molecular dynamic viscosity, d is the distance from the field point to the nearest wall, and $\Omega = \sqrt{2W_{ij}W_{ij}}$ is the vortices magnitude, where

$$W_{ij} = \frac{1}{2} \left(\frac{\partial u_i}{\partial x_j} - \frac{\partial u_j}{\partial x_i} \right) \quad (5)$$

Lastly, the model constant are:

$$\begin{aligned} \sigma_{k1} &= 0.85 & \alpha_{\omega 1} &= 0.5 & \beta_1 &= 0.075 \\ \sigma_{k2} &= 1.0 & \alpha_{\omega 2} &= 0.856 & \beta_2 &= 0.828 \\ \beta^* &= 0.09 & k &= 0.41 & \alpha_1 &= 0.31 \end{aligned}$$

2.2 Transition Model

The $k-\omega$ SST transition model (Menter, F.R, 2004) as implemented within the RANS equations; solves for four transport equations, such as the turbulent kinetic energy (k), specific turbulence dissipation rate (ω), intermittency (γ), and the transition onset momentum thickness Reynolds number ($\text{Re}_{\theta t}$) equations.

The correlation between γ transport equation and $\widetilde{\text{Re}}_{\theta}$ transport equation are based transition model developed by Menter (2004). This framework is for the implementing empirical correlations based transition criteria in general purpose flow solvers, where, structured, unstructured and parallelized solvers can be used together (Niels N. Sørensen, 2009). The constancy of this model is two transport equations, one for intermittent γ and one for the local transition onset momentum thickness Reynolds number $\widetilde{\text{Re}}_{\theta t}$. Mostly, the model relates the local momentum thickness Reynolds number Re_{θ} to the critical value $\text{Re}_{\theta c}$, and switches on the intermittency production when the Re_{θ} is larger than the local critical value. Based on series of zero pressure gradient flat plate boundary layers, Sørensen (2008) have been

determined the expressions for two missing correlation functions relating Re_{θ_c} and F_{length} to \overline{Re}_{θ_t} . The equation dependency of the two correlations is approximated by the following expression:

$$Re_{\theta_c} = \beta \left(\frac{\overline{Re}_{\theta_t} + 12000}{25} \right) + (1 + \beta) \left(\frac{7 \cdot \overline{Re}_{\theta_t} + 100}{10} \right) \quad (6)$$

$$F_{length} = \min \left[150 \cdot \exp \left[- \left(\frac{\overline{Re}_{\theta_t}}{120} \right)^{1.2} \right] + 0.1, 30 \right] \quad (7)$$

Where β is a blending function defined as:

$$\beta = \tanh \left[\left(\frac{\overline{Re}_{\theta_t} - 100}{400} \right)^4 \right] \quad (8)$$

Figure 1 shown good agreement comparing between the present correlation for Re_{θ_c} with the two correlations proposed by Toyoda et al (2007) and Pettersson et al. (2008) at low Re_{θ_t} . Toyoda et al. stated in his paper that the expression for the F_{length} parameter has dimension of length, and not a dimensionless quantity as it should be. A direct comparison of the expression of Toyoda et al. and the present F_{length} parameter therefore is not possible, other way round the correlation proposed by Pettersson et al. show good agreement, shown in Figure 1.

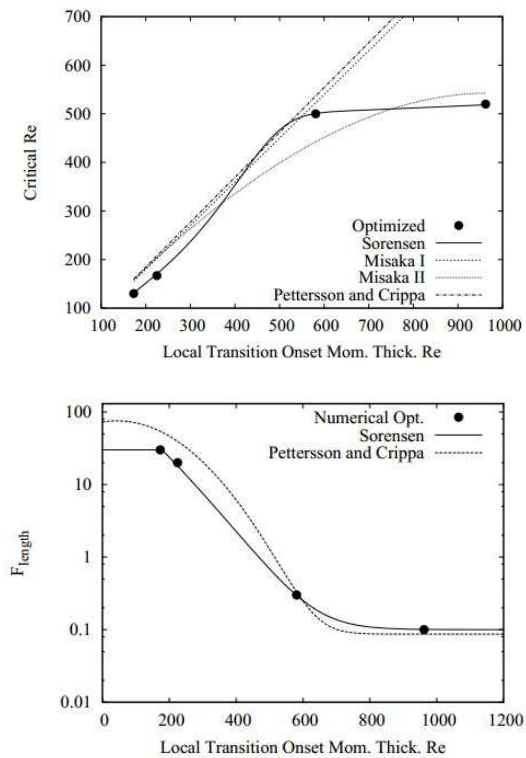


Figure 1: Comparison between the four target points from the optimization and different correlation functions.

Note that, in the case of zero shear where there is no production in the far field, as go to the turbulent will decay from the inlet value. It is shown in Eqn. 10, the farfield value can be estimated to control the level of turbulent kinetic energy at the boundary layer edge, reference (R.B Langtry, 2006):

$$k = k_{inlet} (1 + \omega_{inlet} \beta t)^{-\frac{\beta^*}{\beta}}, \quad (9)$$

where $\beta = 0.09$, and $\beta^* = 0.828$

3.0 AXIAL, NORMAL, LIFT, AND DRAG FORCE DIRECTIONS PROCEDURE

The force coefficient F_x and F_y are parallel and perpendicular to the chord line of the blade, whereas the more usual coefficient F_L and F_D are defined with reference to the direction of the free-stream airflow. (E.L Houghton, 2013)

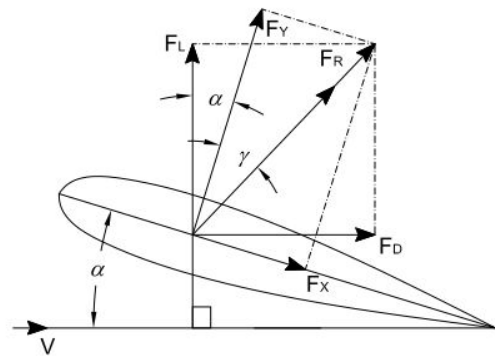


Figure 2: Definition: axial, normal, lift, and drag force directions.

The conversion from one pair of coefficient to the other may be carried out with reference to Figure 7 which is F_R , the coefficient of the resultant aerodynamic force, act at an angle γ to F_Y . F_R is the result both of F_X and F_Y and of F_L and F_D : therefore, based on the Figure 2, it can defined that

$$F_L = F_R \cos(\gamma + \alpha) = F_R \cos \gamma \cos \alpha - F_R \sin \gamma \sin \alpha \quad (10)$$

But $F_R \cos \gamma = F_Y$ and $F_R \sin \gamma = F_X$, so

The lift force can be calculated by:

$$F_L = F_Y \cos \alpha - F_X \sin \alpha \quad (11)$$

Similarly, the drag force also can be calculated by:

$$F_D = F_R \sin(\gamma + \alpha) = F_Y \sin \alpha + F_X \cos \alpha \quad (12)$$

And finally, the coefficients are given by the relationships

$$\text{Lift coefficient, } C_L = \frac{F_L}{\frac{1}{2} \rho V^2 S} \quad (13)$$

$$\text{Drag coefficient, } C_D = \frac{F_D}{\frac{1}{2} \rho V^2 S} \quad (14)$$

4.0 DESCRIPTION OF THE PHYSICAL MODEL

4.1 Airfoil Blade

The model was based on the actual scale of a generic model of the tail rotor blades Bell 206B helicopter, as shown in Figure 3. The blade was 720 mm overall length and has 134 mm length of the chord.

The airfoil profile of the blade is near similar to NACA 0012 series, with maximum thickness 12% at 33% chord as shown in Figure 4. In this study, 3D CAD geometry blade model as shows in Figure 5 has been generated in AutoCAD will be used in this simulation.



Figure 3: The generic used model of tail rotor blade Bell B206

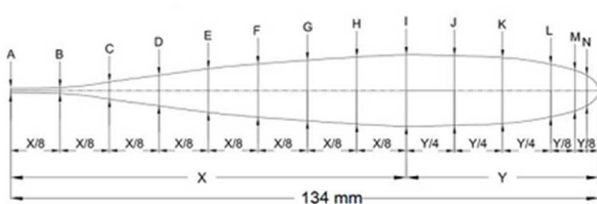


Figure 4: Airfoil profile of tail rotor blade.

4.2 Solution Grid

The 3D CAD model of the tail rotor blade was imported in the Design Modeler and the 3D block domain has been generated, as shown in Figure 6. Figure 7 and Figure 8 shows the meshing of 3D block structured hexahedral grids were created in the pre-processor ICEM-CFD. This pre-processor is the computer program were can be used to generate structured or unstructured meshes consisting of quadrilateral, triangular or tetrahedral elements of 2D and 3D models. In this case, the mesh for the blade model is an unstructured type, consisting 2,536,280 cells and 630,727 nodes.

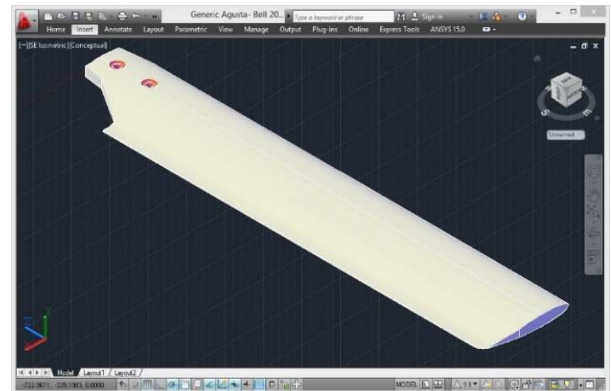


Figure 5: The 3D CAD model of tail rotor blade from Bell B206 using AutoCAD.

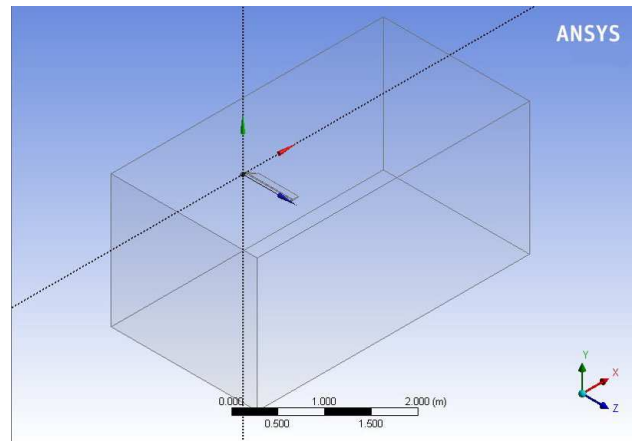


Figure 6: 3D block geometry in ANSYS Design Modeler

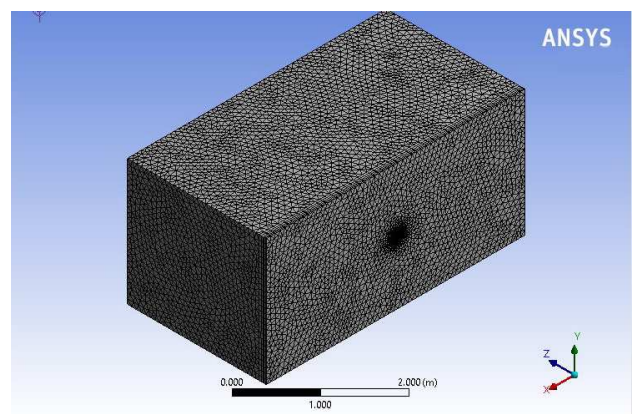


Figure 7: 3D block structured hexahedral mesh

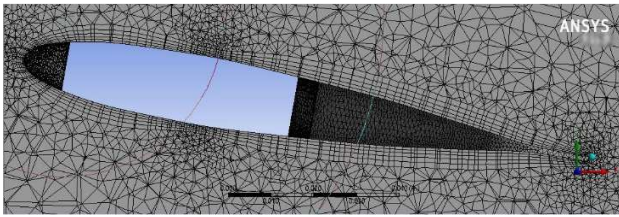


Figure 8: Close-up view of the meshing around the blade model

5.0 SIMULATION METHOD

In order to validate the present simulation process, the operating conditions are mimicked to match the operating conditions of the experimental works conducted previously in the Universiti Teknologi Malaysia- Low Speed Tunnel (Firdaus, 2015). The velocity inlet (Figure 9) for the simulation were set from 5 m/s to 40 m/s, corresponds to a Reynolds number based on airfoil chord from 0.419×10^5 to 3.352×10^5 and angle of attack of 0, 5, 10, 12, 15, 18, 20, and 25 degrees. The free stream temperature is 298.65 K, which is the same as the surrounding air temperature. The density of the air at the given temperature is $\rho = 1.17 \text{kg/m}^3$ and the viscosity is $\mu = 1.859 \times 10^{-5} \text{kg/m-s}$.

In this study, it is assumed that inlet velocity is same turbulent as pressure outlet. So, for velocity inlet boundary condition turbulent intensity is considered 5% and for pressure outlet boundary is also considered 5% as recommended by ANSYS, which state the inlet boundary condition turbulence intensities is ranging from 1% to 5%. In addition, turbulent viscosity was set to 10 for a better approximation of the problem as recommended by ANSYS.

Table 1 shows the ANSYS FLUENT setup for $k-\omega$ SST transition model before the simulation are executed:

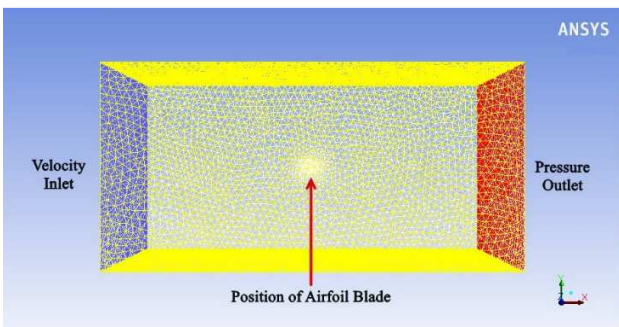


Figure 9: Domain mesh of FLUENT simulation

SOLUTION SETUP	GENERAL	
	Solver Type	Pressure-Based
	Velocity Formulation	Absolute
	Time	Steady
	MODELS	
	Viscous	Transition SST
	MATERIALS	
	Air	Density = 1.17 kg/m^3 Viscosity = $1.859 \times 10^{-5} \text{ kg/m-s}$
	BOUNDARY CONDITIONS	
	Gauge Pressure	0 Pascal
	Temperature	298.65 K
	Operating Pressure	101325 Pascal
	Turbulence	
	Specification Method	Intermittency, Intensity and Viscosity Ratio
	Intermittency	1
Turbulent Intensity	5 %	
Turbulent Viscosity Ratio	10	
SOLUTION	SOLUTION METHODS	
	Pressure-Velocity Coupling	
	Scheme	Coupled
	Spatial Discretization	
	Gradient	Least Square Cell Based
	Pressure	Second Order
	Momentum	Second Order Upwind
	Turbulent Kinetic Energy	Second Order Upwind
	Momentum Thickness Re	Second Order Upwind
	SOLUTION CONTROLS	
	Explicit Relaxation Factors	
	Momentum	0.75
	Pressure	0.75
	Density	1
	Body Force	1
Turbulent Kinetic Energy	0.8	
Momentum Thickness Re	0.8	
Turbulent Viscosity	1	

Table 1: ANSYS FLUENT setups for $k-\omega$ SST transition model

6.0 RESULT AND DISCUSSION

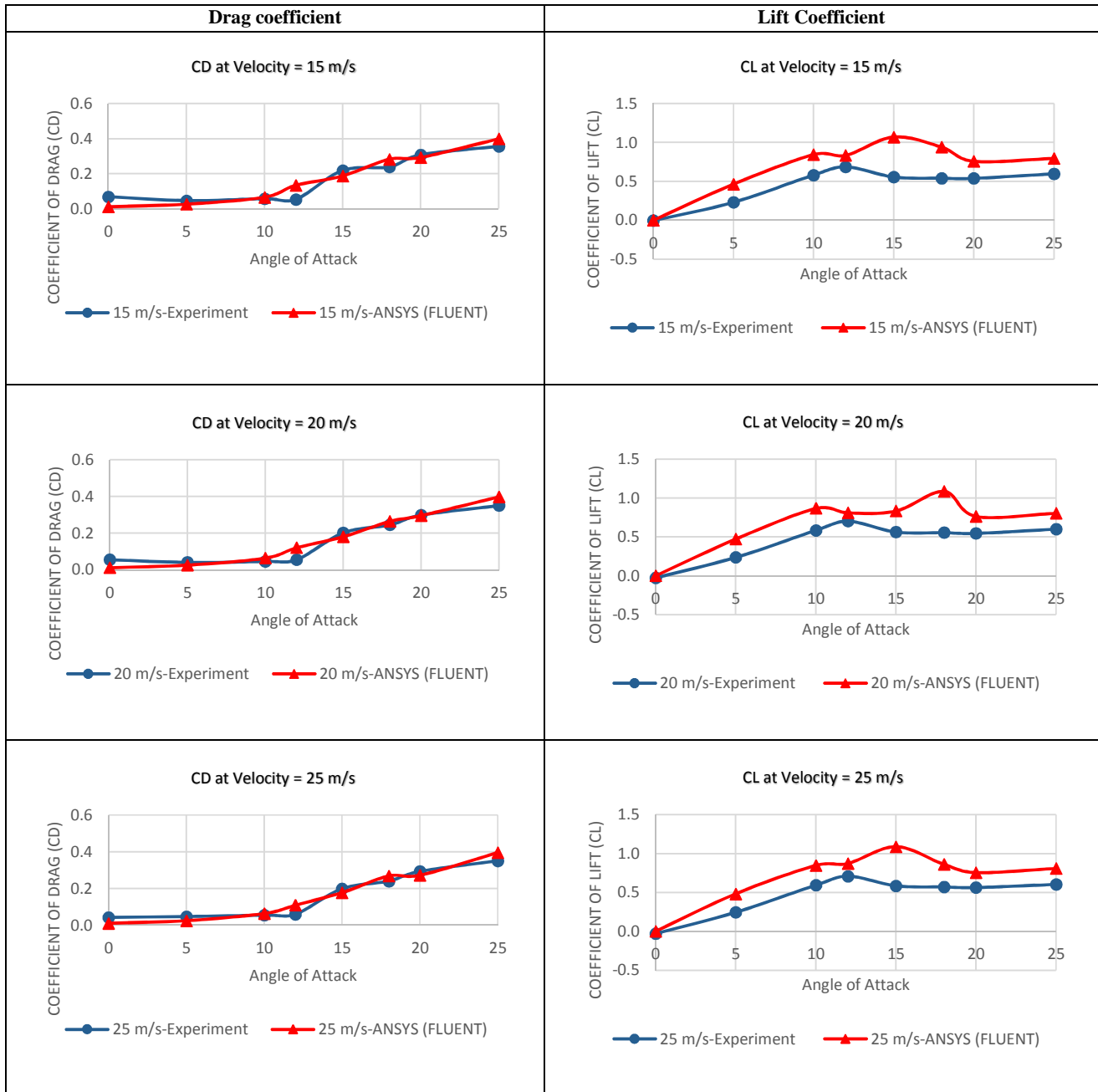


Figure 10 (a): Drag and lift coefficient of the blade model at different air speed and angles of attack.

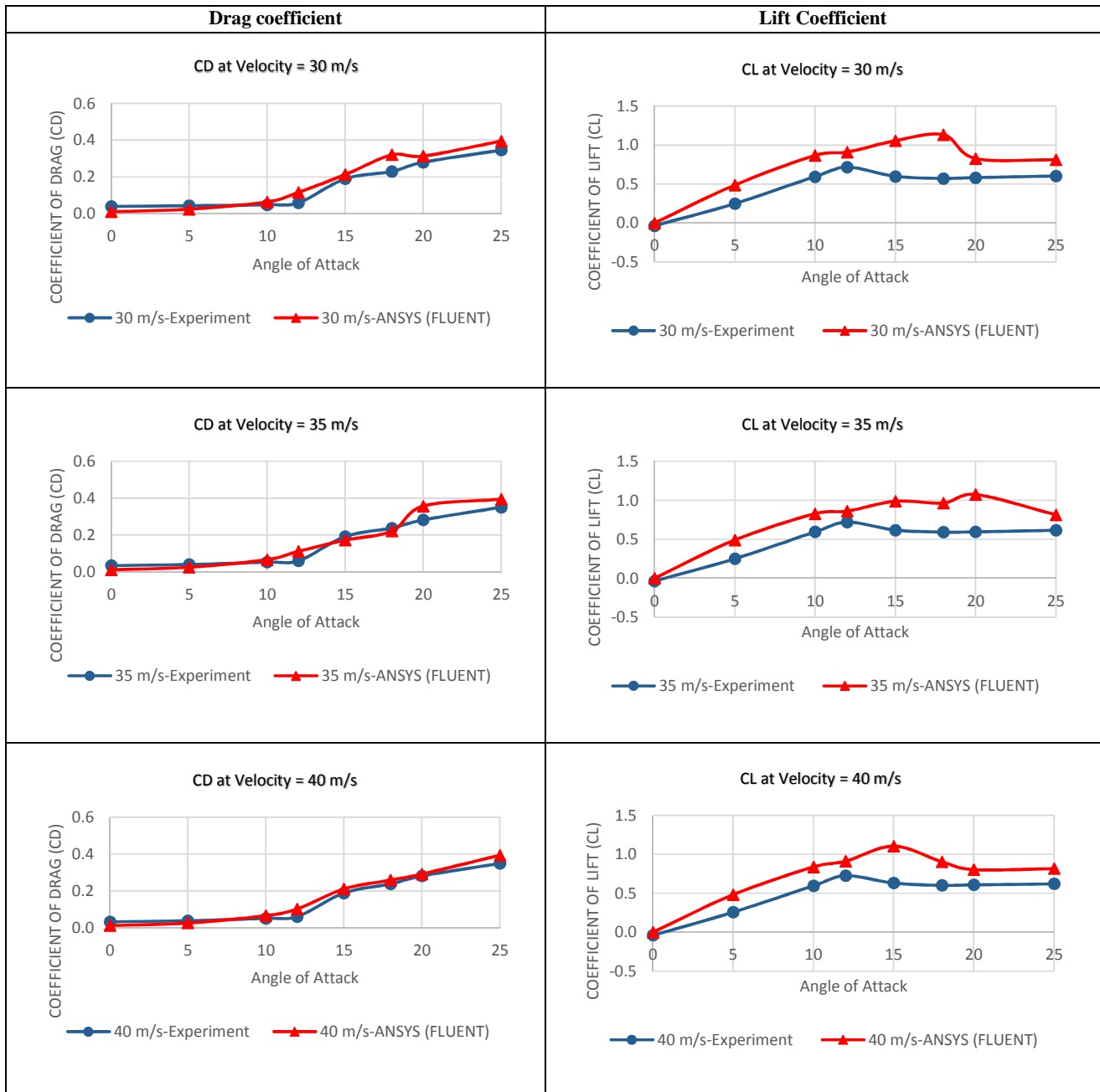


Figure 10 (b): Drag and lift coefficient of the blade model at different air speed and angles of attack.

Figure 10 (a) and (b) show the comparison of C_D and C_L values between numerical and experimental works for variation of wind speed and angle of attack.

It is observed that the numerical results give reasonably good tendency against the ones from experimental works. This tendency starts improving with an increment of Reynolds number. The

results for the drag coefficient (C_D) show that there is quite good agreement between the experiment and computational results. On the contrary, the prediction of computation for the lift coefficient (C_L) slightly overshoot against the experimental results.

Although the predictions of $k-\omega$ SST transition model do not fully agree, the relative agreement is still reasonable as both

computational and experimental, at least agrees at the trend of the lift and drag coefficients as the Reynolds number changes.

In case for low Reynolds number flow conditions, predicting the drag coefficient becomes even more problematic, since low Reynolds number airfoils normally exhibit laminar separation bubbles, which are known to significantly affect the performance of an airfoil blade. As for increasing the Reynolds number, the ability of prediction of drag and lift coefficient becomes easier for the flow solvers because the flow is no longer laminar, and turbulent boundary layer is effective on the surface of the airfoil blade beginning from the leading edge.

7.0 CONCLUSION

The computational analysis of three dimensional (3D) flow over the generic model of Bell 206B helicopter tail rotor blades using ANSYS FLUENT based on $k-\omega$ SST transition model has been demonstrated. The solutions obtained from FLUENT simulation are compared with the experimental result (Firdaus, 2015), and it is noted that the prediction gives a good agreement for the inclination of the lift coefficient and drag coefficient, although over predict at low Reynolds number flow conditions. Nevertheless it is conceded that there could be discrepancies with the exact data of the 206B rotor tail blade since several assumptions had been made, and also due to some limitations of experimental and simulation works.

REFERENCE

1. Niels N. Srensen, 2009, "3D CFD Computations of Transitional Flows Using DES and A Correlation Based Transition Model". Risø DTU. National Laboratory for Sustainable Energy. Technical University of Denmark
2. Ünver Kaynak Samet Çaka Çakmakçioğlu and Mustafa SerdarGenç, 2012, "Transition at Low-Re Numbers for some Airfoils at High Subsonic Mach Numbers". Low Reynolds Number Aerodynamics and Transition, InTech Europe, pp. 79-96.
3. Giles, Michael B. and Mark Drela, 1987, "Two-Dimensional Transonic Aerodynamic Design Method", AIAA Journal, vol. 25, no. 9, Sept. 1987, pp. 1199-1206.
4. Wilcox, D.C., 1994, "Simulation of Transition with a Two-Equation Turbulence Model", AIAA Journal, Vol. 32, No. 2, pp. 247-255.
5. Suzen, Y. B. and Huang, P.G., 2000, "Modeling of Flow Transition Using an Intermittency Transport Equation", ASME Journal of Fluid Engineering, Vol. 122, pp. 273-284.
6. F. R. Menter, R. B. Langtry, S. R. Likki, Y. B. Suzen, P. G. Huang, and S. Volker, 2004, "A Correlation-Based Transition Model Using Local Variables, Part I - Model Formulation". In Proceedings of ASME Turbo Expo 2004, Power for Land, Sea, and Air, Vienna, Austria, June 14-17 2004. ASME. GT2004-53452.
7. M. Strelets, 2001, "Detached Eddy Simulation of Massively Separated Flows". AIAA Paper 2001-0879, Russian Scientific Center "Applied Chemistry" St. Petersburg.
8. Firdaus, Jaswar Koto, I.S Ishak, M.S Ammoo, 2015, "Wind Tunnel Test on Generic Agusta-Bell 206B Helicopter Tail Rotor Blades". Journal of Aeronautical -Science and Engineering-, Vol 1, pp. 1-6.
9. Tousif Ahmed , Md. Tanjin Amin , S.M. Rafiul Islam & Shabbir Ahmed, 2013, "Computational Study of Flow Around a NACA0012 Wing Flapped at Different Flap Angles with Varying Mach Numbers". Global Journal of Researches in Engineering General Engineering. Volume 13 Issue 4 Version 1.0.
10. Menter, F.R., Langtry, R.B., Likki, S.R., Suzen, Y.B., Huang, P.G. and Völker, s. , 2004, "A Correlation Based Transition Model Using Local Variables: Part I-Model Formulation ASME-GT2004-53452, Proceedings of ASME Turbo Expo 2004, Vienna, Austria, pp. 57-67.
11. E.L. Houghton, P.W. Carpenter, Steven Collicott and Dan Valentine. 2012. Aerodynamics for Engineering Students (Sixth Edition). Butterworth-Heinemann. Page: 54-55.
12. A. Toyoda, T. Misaka, and S. Obayashi, 2007, "An Application of Local Correlation-Based Transition Model to JAXA High-Lift Configuration Model". AIAA Paper 2007-4286, June 2007.
13. K. Pettersson and S. Crippa, 2008, "Implementation and Verification of a Correlation Based Transition Prediction Method". AIAA Paper 2008-4401.
14. R. B. Langtry, J. Gola, and F. R. Menter, 2006, "Predicting 2D Airfoil and 3D Wind Turbine Rotor Performance using a Transition Model for General CFD Codes". AIAA-paper-2006-0395.